doi:10.1017/S1431927614004255
Microsc. Microanal. 20 (Suppl 3), 2014

Understanding the Role of Potassium Doping in PbTe-PbS Thermoelectrics

H. J. Wu,[1] L.-D. Zhao,[2] F.S. Zheng,[1] D. Wu,[1] Y. L. Pei,[3] X. Tong,[1] and J. Q. He[1,*]

[1.] Department of Physics, South University of Science and Technology of China, Shenzhen 518055, China
[2.] Department of Chemistry, Northwestern University, Evanston, Illinois 60208, USA
[3.] School of Materials Science and Engineering, Beihang University, Beijing 100191, China

Thermoelectric materials, capable of scavenging electric power from sources of waste heat, are one of promising choices for relaxing global energy problems [1]. However, the low energy conversion efficiency limits such smart materials to put into use widely. We achieved an excellent thermoelectric performance in 2.5% K doped $PbTe_{0.7}S_{0.3}$ sample: one of the highest dimensionless figure of merit *(ZT)* of 2.2 at 923 K and the highest energy conversion efficiency of ~20.7% (i.e. the highest average *ZT* of 1.56) for non-segmented thermoelectric devices. Hopefully, this work highlights a realistic prospect of wide thermoelectric application with high *ZT* (above 3). In order to obtain the above high performance, we subtly tuned K doping level in spinodal decomposed PbTe0.7S0.3 system to firstly realize a simultaneous enhancement of electrical conductivity and Seebeck coefficient and a reduction of thermal conductivity [2]. Accordingly, a precise characterization and analysis of microstructure as they relate to thermoelectric performance are vitally important for the fundamental understanding of this peculiar thermoelectric material. **The presentation will cover S/TEM microscopy and microanalysis strategy to unravel microstructural influence on thermoelectric properties and associated phenomena.**

The nominal *x%* K doped $PbTe_{0.7}S_{0.3}$ composition spinodally decomposes into two phases: PbTe and PbS. Meanwhile, mesoscale grains can be obtained via spark plasma sintering. Thus high density of grain/phase boundaries can be got, as shown in **Fig. 1(a) and (b).** Lattice images and schematic maps in **Fig. 1(c-f)** reveal that both grain/phase boundaries are semi-coherent and full of edge dislocations and strains. Besides the mesoscale grain regions, nanoscale precipitates can always be found widely but distinctly inside PbTe and PbS regions. **Fig. 2** gives microstructure evolution of precipitates as a function of K doping in PbS and PbTe regions in *x%* K doped $PbTe_{0.7}S_{0.3}$ samples. For PbS regions **(Fig. 2(a-d)),** with the increase of K doping, the density of precipitates is almost unchanged, while the morphology changes a lot, from platelet-like for lowly K doping ($x<2.5$) to cubical one for certain K doping ($x=2.5$), and finally to sticking-sphere for highly K doping ($x>2.5$). On the contrast, the density and size of precipitates in PbTe regions increase with the increase of K doping, **Fig. 2(e-g).** The underlying mechanism of the above evolutions is the solubility difference of K in PbTe, PbS and PbTeS compounds. **Fig. 3** is detailed structural analysis of the cubical precipitates of 2.5% K doped $PbTe_{0.7}S_{0.3}$. Diffraction patterns in **Fig. 3(a), 3(c) and 3(e)** show two types of superlattices besides the main reflections, i.e., near-1/3 (2,0,0) and near-(1,1/3,0) supperlattices, from different precipitates. Correspondingly, lattice images of cubical precipitates in real space exhibit a 3-layers period, **Fig. 3(b) and 3(d).** Furthermore, the near-1/3 superlattices can be expressed as $(1/3-\varepsilon)(2, 0, 0)$ or $(1/3-\varepsilon)(0, 2, 0)$ accurately due to the substitution of Te on S sites, with deviation parameter ε, **Fig. 3(g).** It is clearly shown that superlattices are due to chemical ordering in cubical $PbTe_{1/6}S_{5/6}$ precipitates, as shown in **Fig. 3(f).** Therefore, nanoscale precipitates combining with long-wavelength phonon scattering centers (mesoscale grain/phase boundaries), and short-wavelength phonon scattering centers (atomic-scale

dislocation/strain/point defects), established a hierarchical architecture to effectively scatter phonons with all lengths.

Reference:
[1] He J, Kanatzidis MG, Dravid VP. Materials Today **16** (2013), p.166.
[2] Wu. HJ, et al. Submitted 2014.

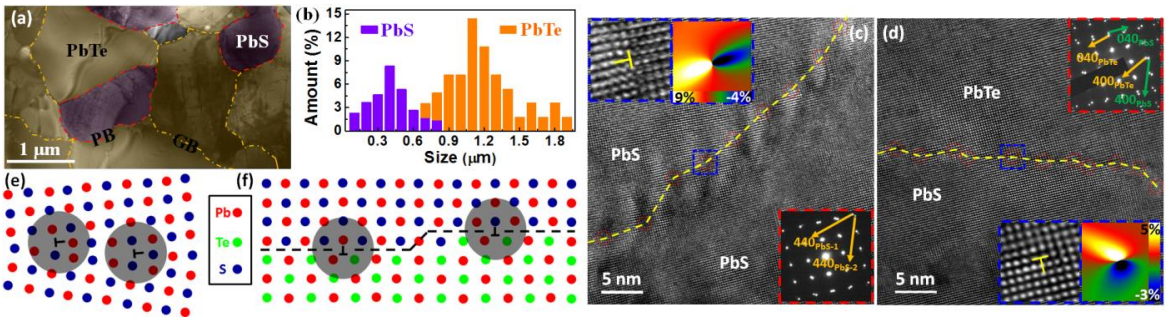

Figure 1. (a) TEM image reveals mesoscale PbTe/PbS grains; (b) Grain size distribution histogram; (c) and (d) Lattice image of PbS/PbS grain boundary and PbTe/PbS phase boundary, respectively. ED patterns, enlarged images for edge dislocations and GPA analysis images are inserted; (e) and (f) schematic figures showing the grain and phase boundary, respectively.

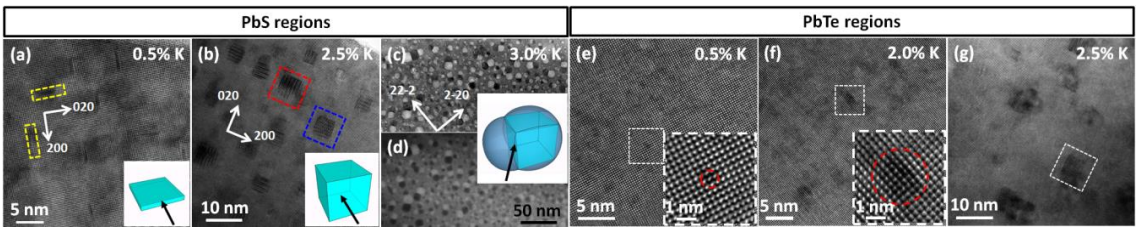

Figure 2. (a-d) Images showing platelet-like, cubical, and sticking-sphere precipitates in PbS regions for 0.5% K, 2.5% K and 3.0% K samples, respectively. (e-g) Images showing roughly homogeneous contrast with only some weak-contrast particles, low density of precipitates with a grown size, and high density of larger precipitates for 0.5% K, 2.0% K and 2.5% K samples, respectively.

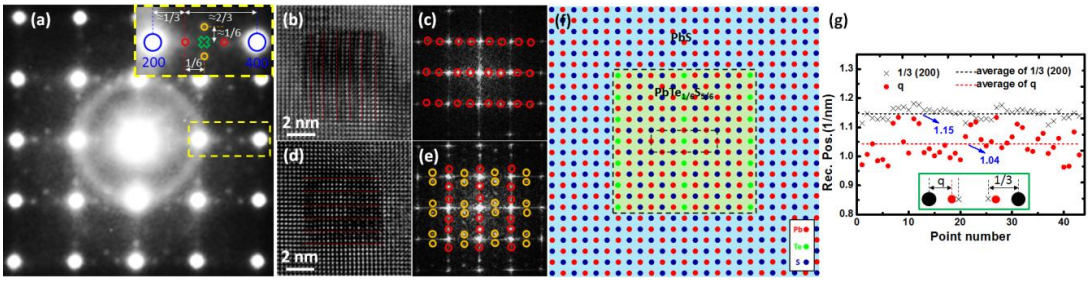

Figure 3. (a-g) Structural analysis of cubical precipitates of 2.5% K sample: (a) ED pattern of Figure 2(b), showing two types of superlattices besides the main reflections, i.e., near-1/3 (200) and near-(1 1/3 0) superlattices; (b) and (d) Enlarged image of precipitates, 3-layers period is marked; (c) and (e) IFFT images of (b) and (d), the respective superlattices are marked; (f) The atomic modeling of the cubical precipitates, the unit cell of superlattices is marked; (g) Statistical reciprocal positions of near-1/3 (200) superlattices (red dots) and the 1/3 (200) (black crosses, non-existed) are counted, and their average values are also shown.

https://doi.org/10.1017/S1431927614004255 Published online by Cambridge University Press